The effect of natural fracture heterogeneity on hydraulic fracture performance and seismic response in shale and coal formations

Yildirim, B.; Cao, W.; Durucan, S.; Korre, A.; Wolf, K. H.; Bakker, R.; Barnhoorn, A.

Publication date
2018

Document Version
Final published version

Published in
52nd U.S. Rock Mechanics/Geomechanics Symposium

ARMA 18–277

The Effect of Natural Fracture Heterogeneity on Hydraulic Fracture Performance and Seismic Response in Shale and Coal Formations

Yildirim, B., Cao, W., Durucan, S., Korre, A.

Department of Earth Science and Engineering, Royal School of Mines, Imperial College London, London SW7 2AZ, United Kingdom.

Wolf, K.H., Bakker, R., Barnhoorn, A.

Delft University of Technology, Department of Geoscience and Engineering, Delft University of Technology, Delft, the Netherlands

ABSTRACT: Two 0.3 m × 0.3 m × 0.3 m cubic blocks of shale and coal were used for hydraulic fracturing experiments under true tri-axial stress conditions. The shale block used was highly homogeneous and without visible fractures, while the coal block contained a host of natural fractures. The mechanical and hydraulic properties of both rocks were characterized through multi-stage triaxial tests, Brazilian disk tests, and porosity and permeability measurements. A true tri-axial rock testing machine equipped with loading, pump and acoustic systems was used in the experiment. The acoustic system uses 48 transducers with active sources to repetitively generate and receive ultrasonic P/S wave pulses to reveal fracture initiation and growth. Before the experiment, initial seismic response of both blocks was recorded under hydrostatic stress conditions to characterize anisotropy and heterogeneity of the blocks as reference. Silicon oil was injected centrally into both blocks to create a hydrofracture under deviatoric stress conditions and the load, displacement, pump pressure and volume, and seismic response during the injection process were recorded. Results from two blocks are being compared in terms of hydrofracture geometry and seismic features.

1. INTRODUCTION

Hydraulic fracturing is both an efficient and widely used technique to enhance permeability and increase productivity in unconventional gas reservoirs and in releasing gas pressure to combat coal and gas outburst hazards in coal mines. In this context, understanding fracture initiation, propagation, and its interaction with other fractures, plays a significant role both in estimation of simulated rock volume (SRV) in unconventional reservoirs and in prevention of mining hazards.

Including the rock properties and the operational procedures, there are different parameters affecting the hydraulic fracturing performance. There is a considerable amount of research on understanding the hydraulic fracture behaviour in different rock formations (Guo *et al*., 1993; Akrad *et al*. 2011**;** Ding *et al*., 2012; Fischer and Warpinski, 2012; Zhang *et al*., 2013; Padin *et al*. 2014; Li *et al*., 2015; Stoechert *et al*., 2015; Liang *et al*., 2017; Zhu *et al*., 2017). However, most of the experimental research was conducted on isotropic and homogeneous rock or synthetic samples, which resulted in unrealistic estimations.

As the hydraulic fracture behaviour is highly affected by the presence of natural fractures and bedding planes, it is of great importance to understand the fracture initiation and propagation behaviour in heterogeneous rock formations for the performance assessment and effective control of the fracturing process. The findings of previous experimental research on NF/HF interaction have shown that the effects of orientation, ubiquity, and mechanical and geometrical properties of natural fractures on hydraulic fracture performance are significant (Zoback *et al*., 1977; Blanton, 1982; Warpinski and Teufel, 1987; Zhou *et al*., 2008, Zhou and Chengjin, 2011; Dehghan, 2015; Hou *et al*., 2016; Al Tammar *et al*., 2017; Huang and Liu, 2017; Peng *et al*., 2018). Nevertheless, there still is the need for further research towards establishing an understanding on how mechanical and hydraulic properties, as well as fracture intensity, influence the hydraulic fracture propagation and associated seismic response.

This research aimed at conducting hydraulic fracturing experiments on two 0.3 × 0.3 m × 0.3 m cubic blocks, one shale and one coal, under true tri-axial stress conditions. The shale block used was highly homogeneous and without visible fractures, while the coal block contained a host of natural fractures. Results from two blocks have been compared in terms of seismic features on the basis of seismic wave velocity, wave propagation and attenuation.

2. EXPERIMENTAL METHODOLOGY

The shale samples used in this research were collected from the Hope Cement Works shale quarry in Derbyshire, UK and the large coal blocks used to prepare the samples were obtained from a coal mine in Poland. As the rock properties play a significant role in hydraulic fracture propagation, mechanical, elastic, and hydraulic properties of both the shale and coal samples were obtained through multi-stage triaxial tests, Brazilian disk tests, and porosity and permeability measurements in the laboratory (Table 1).

Table 1. Mechanical, elastic, and hydraulic properties of shale and coal samples.

Sample	Tensile Strength (MPa)	UCS (MPa)	Young's Modulus (GPa)	Poisson's Ratio	Permeability (10^{-15} m^2)	Porosity (%)
Shale	8.3	82.0	15.6	0.29	0.1	1.88
Coal	0.47	9.2	3.1	0.21	1.0	2.00

2.1. True-triaxial Testing System

A true-triaxial cell (TTSC) equipped with piezoelectric transducers, referred to as active sources, was used for the hydrofracturing experiments. The true-triaxial cell at TU Delft Geoscience Laboratory can accommodate 0.3m cubic samples and can hold up to 48 transducers in total with 8 ports available on each face (Fig. 1).

Transducer alignment used in the experiments is presented in Fig. 2. Based on the findings and suggestions of previous hydraulic fracturing experiments conducted at TU Delft (Savic, 1995; Weijers, 1995; Groenenboom, 1998; Van de Ketterij, 2001; Meng, 2010), all 48 transducers were used in the research. Each transducer could function both as a source and receiver, and 960 different source-receiver combinations were possible, including straight transmission, oblique transmission, and diffraction pairs. In total, there were 24 P-wave and 24 S-wave transducers in the given alignment. Throughout the ultrasonic measurements, the transmission and diffraction waves were used for the interpretation of the hydraulic fracturing experiments.

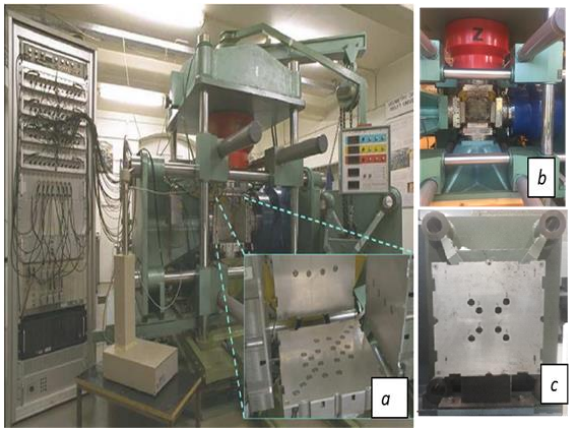

Fig. 1. (a) External view of the TTSC testing unit, (b) the loading plates attached, and (c) transducer insert ports.

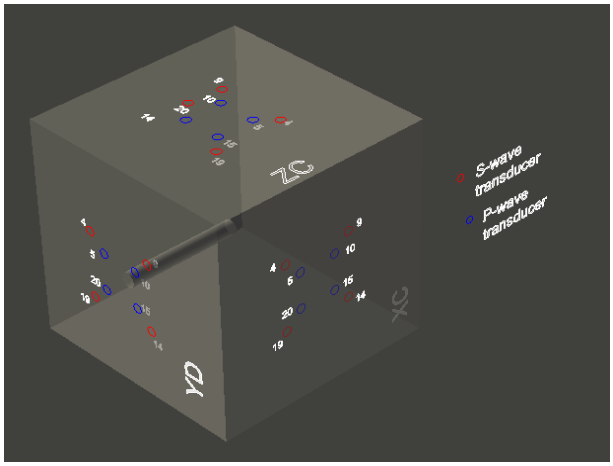

(a)

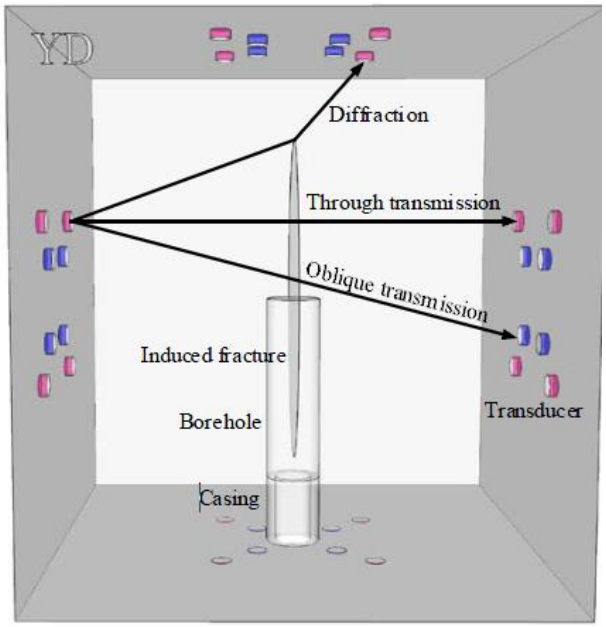

(b)

Fig. 2. (a) Alignment of P-wave and S-wave transducers, and (b) transmission and diffraction raypaths.

2.2. *Sample Preparation and Experimental Procedure*

After cutting to size, the rough surfaces of both cubic samples were smoothened to finish the samples with equal size sides. A 23 mm diameter borehole was drilled along the y direction in the shale block. A 150 mm long casing was placed into the wellbore without leaving an open-hole section. A 34 mm diameter borehole was drilled along the z direction in the coal sample and 40 mm short steel casing with a diameter of 23 mm was inserted in the borehole. The borehole assembly was connected to the injection system to inject fluid by a pump. The blocks were then placed in the true-triaxial compression machine and loaded at different stress stages. Three cylinders XC, YC, and ZC independently push the sample against three fixed plates, XD, YD, and ZD.

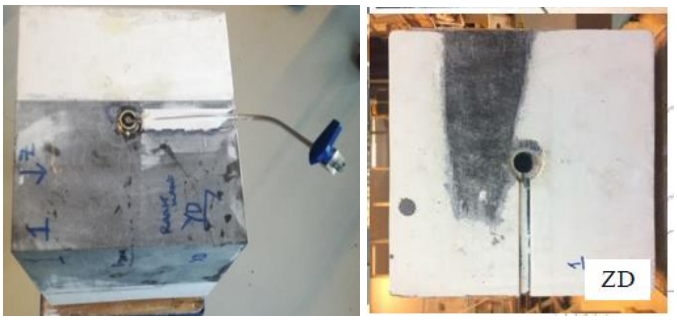

(a)……..(b)

Fig. 3. Borehole assemblies for (a) shale and (b) coal blocks.

In order to obtain seismic wave profiles under different confinements, a stepwise loading procedure was implemented before the hydraulic fracturing experiments, results of which are presented in Section 3.

During the hydraulic fracturing experiments, equal load was applied on each side of the cubes until reaching the final stress state. At the final stress level, stress magnitude in the x direction was decreased while keeping stress constant in y and z directions. Next, fluid was injected at a constant flow rate of 1 ml/min. Silicon oil was used as the fracturing fluid and the initiation of the induced fracture could be detected by observing the changes in the acoustic measurement data, in particular the increase in amplitude and time delays in propagation of seismic waves.

During the fluid injection stage, the load, pump pressure and seismic response were recorded. Once the fractures are induced, the sample was unloaded following the same stress stages used for the loading case. The samples were then taken out of the true-triaxial cell to observe the induced fractures by naked eye.

3. RESULTS AND DISCUSSION

Fig. 4 presents stress and borehole pressure data against experiment time. The sudden decrease in borehole pressure observed in the figures indicate the initiation of hydraulic fractures in the samples. The fluid injection pressure started to drop from its maximum value at 495 seconds after the start of the injection for the shale sample and at 230 seconds for the coal sample. This suggests that the initiation of a hydraulic fracture in the coal was much easier due to its fractured and weak nature.

Seismic wave profiles of the shale and coal samples were recorded under different hydrostatic stress conditions prior to the hydrofracturing experiments. The results for the direct transmission pair ZC4-ZD4 and the diffraction pair XC14-YC14 are presented in Fig.5 and Fig.6. Arrival times of the seismic waves for the shale sample was not significantly changed under different confining pressures, whereas an increase in the confining pressure resulted in larger amplitudes of the seismic waves for the coal. In addition, a higher confining pressure led to earlier seismic wave arrivals for the coal sample. It was noted that the diffracted seismic wave for the coal sample is much more scattered than those from other raypaths, which is believed to have caused by pre-existing natural fractures (Fig. 6b).

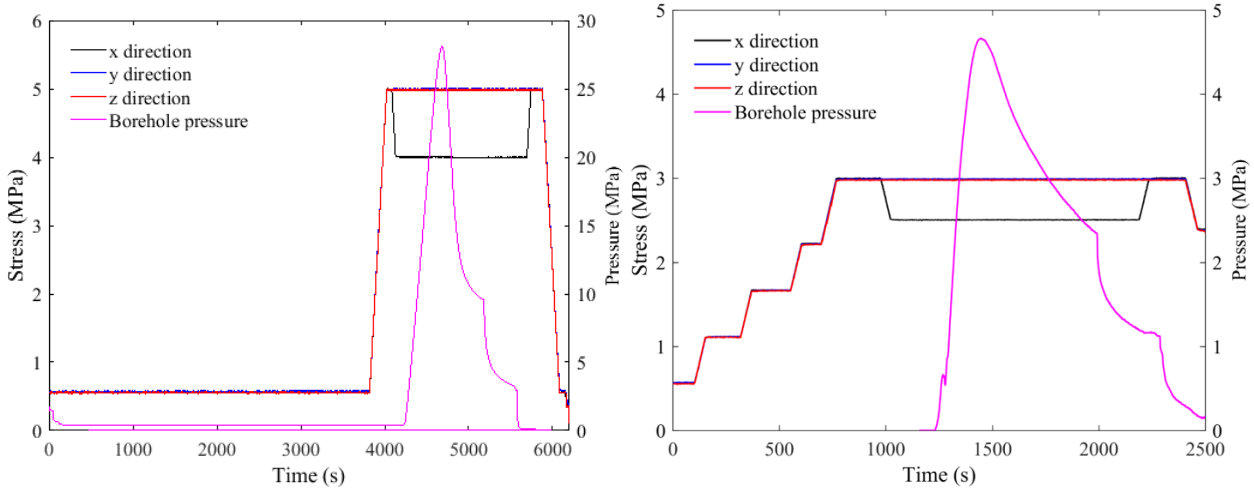

(a) (b)

Fig. 4. Load and pump data results for (a) shale and (b) coal.

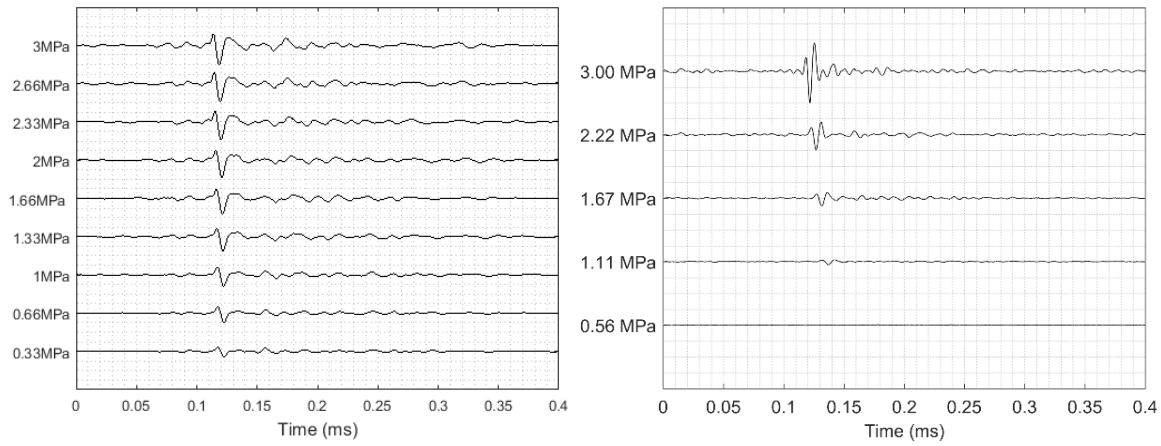

(a) (b)

Fig. 5. Initial seismic response of the (a) shale, and (b) coal samples from the direct transmission transducer pair (ZC4-ZD4) under different confining pressures.

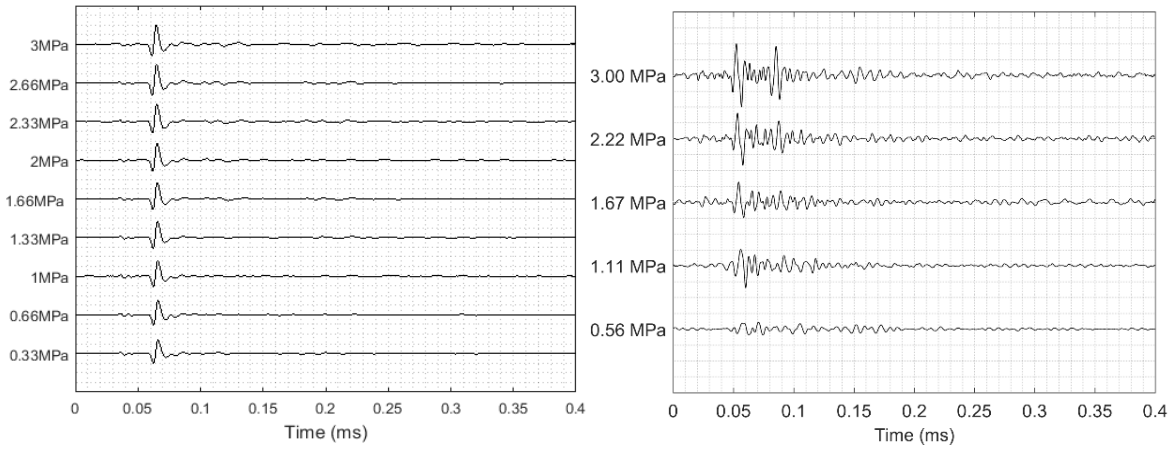

(a) (b)

Fig. 6. Initial seismic response of the (a) shale, and (b) coal samples from the diffraction transducer pair (XC14-YC14) under different confining pressures.

Seismograms and spectrograms for the transmission transducer pair ZC4-ZD4 and the diffraction transducer pair XC14-ZD5 for both samples are presented in Fig.7 and Fig.8. Analysis of the arrival times as well as the amplitudes of the acoustic data confirmed the earlier observations made from monitoring the fluid injection pressure, and that the hydrofracturing of the shale and coal samples took place at 495 seconds and 230 seconds after the start of the injection, respectively. In addition, seismic spectrograms of transmission raypaths could only capture the initiation of the induced fracture, while those of diffracted raypaths could reflect both the fracture initiation and its subsequent interactions with the natural fracture system (Fig. 8b).

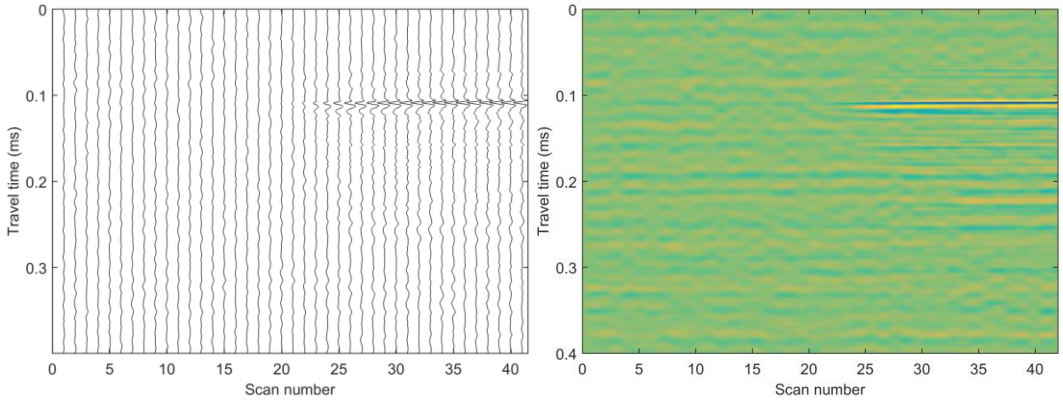

(a)

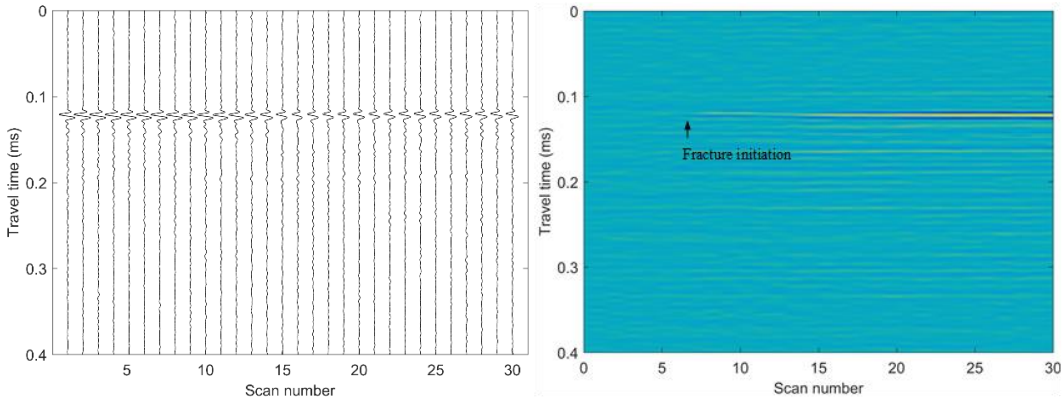

(b)

Fig. 7. Seismograms and spectrograms from the direct transmission transducer pair ZC4-ZD4 for the (a) shale and (b) coal samples.

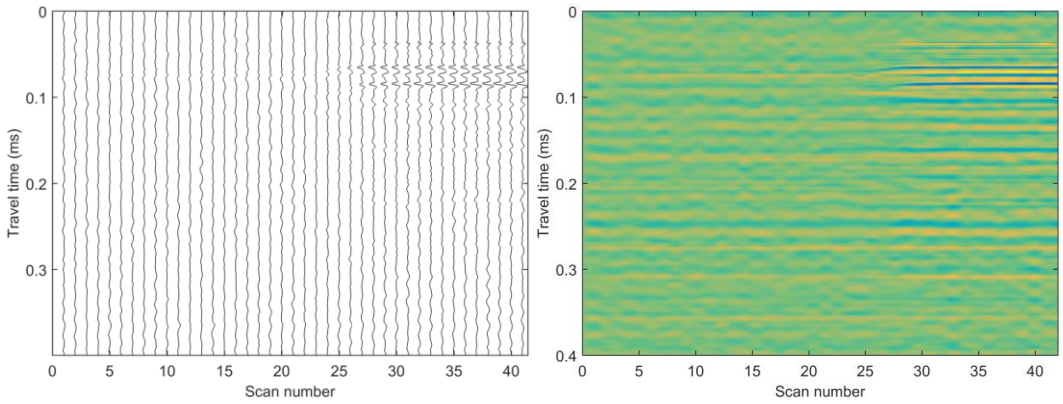

(a)

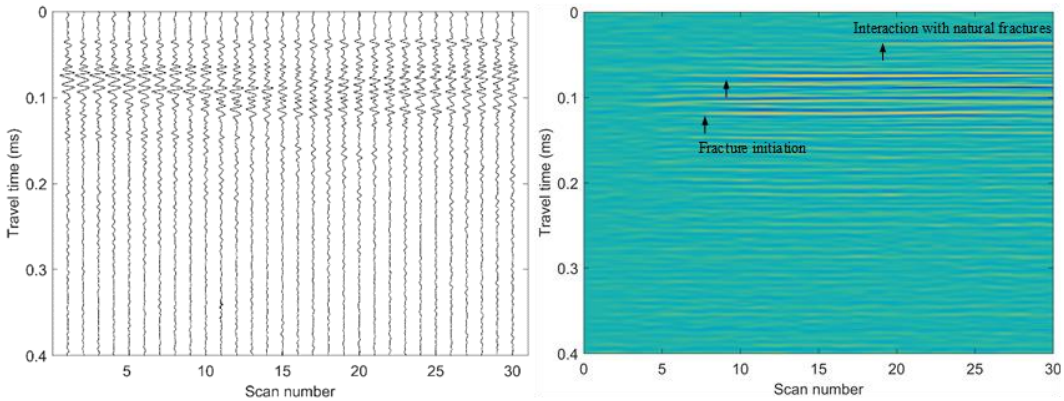

(b)

Fig. 8. Seismograms and spectrograms from the diffraction transducer pair XC14-ZD5 for the (a) shale and (b) coal samples.

Fig. 9 and Fig. 10 present schematic diagrams showing how seismic spectrograms are correlated with propagating fractures in intact and fractured blocks, respectively. An emitted acoustic signal propagates radially from the emitting transducer, and can be reflected or diffracted when encountering obstacles. As a result, the received acoustic signal is the superposition of seismic waves from different raypaths. Before the initiation of the induced fracture in an intact block, two obvious raypaths from the emitting to receiving transducers involve a straight transmitted raypath 1, and a diffracted raypath 2 via the borehole end, as shown in Fig. 9(a). Other raypaths, where steel casing and other pre-existing natural fractures act as diffractors are ignored to simplify the analysis. The generation of the induced hydraulic fracture forms a new raypath 3 where the seismic wave diffracted via the tip of the induced fracture (Fig. 9(b)), leading to the superposition of a new wave component to the received seismic wave. Fig. 9(c) present the seismograms recorded from the same transducer pair on the relatively intact shale block before and after injection, respectively. The seismogram 2 shown in Fig. 9(d), which was processed by subtracting the initial scan from the second one, reflects the impact of the newly introduced raypath 3 as shown in Fig. 9(b). It is a separate, delayed wave packet, similar to the original scan in waveform.

For blocks with embedded natural fractures, the seismic raypaths are similar to those for the intact block before the induced fracture interacts with a natural fracture (Fig. 10(a) and (b)). After coalesce between induced and natural fractures, the fracturing fluid penetrates into the natural fracture and the fluid front act as a diffractor, introducing more raypaths, as illustrated in Fig. 10(c). Even more raypaths may emerge when the fracturing fluid is connected to a natural fracture system. Fig. 10(d) and (e) present the original and processed seismograms of the same transducer pair on the highly fractured coal block over the injection process. It can be seen that the injection-induced diffraction can be treated as a scattered wave packet arriving almost simultaneously as the original acoustic signal.

It is difficult to correlate fluid penetration into each natural fracture branch with induced diffraction waves due to the geometrical complexity of natural fracture networks and the associated multiple reflection and diffraction before reaching receiving transducers. Nevertheless, analysis of recorded seismograms of elastodynamic waves provides a new alternative to detect and analyse the initiation of a hydraulic fracture and its subsequent interaction with the complex natural fracture system inside rock masses. This method might be promising for the analysis of field-scale injection-induced fracture behaviour.

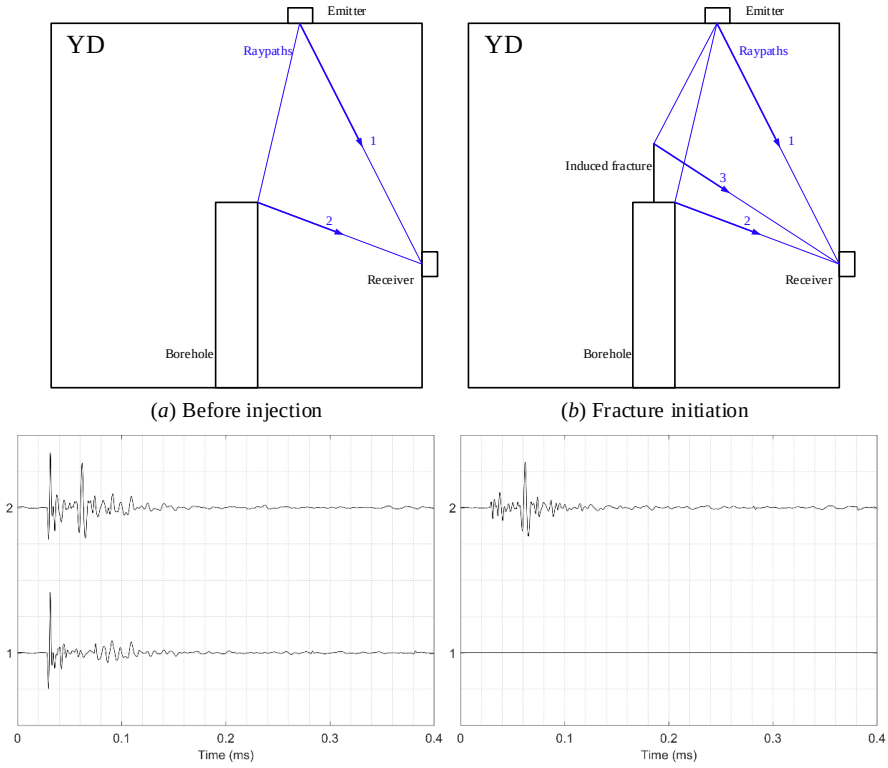

(*a*) Before injection

(*b*) Fracture initiation

(*c*) Original wave profiles (shale, ZC9-XD10, dS)

(*d*) Processed wave profiles by subtracting the first scan from each subsequent scan (shale, ZC9-XD10, dS)

Fig. 9. Interpretation of seismic spectrograms in response to injection to intact blocks.

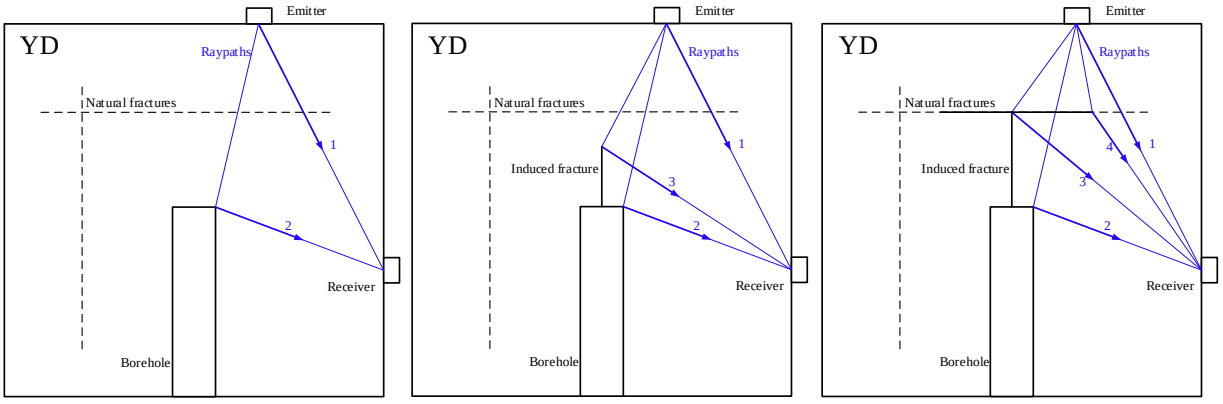

(*a*) Before injection (*b*) Fracture initiation (*c*) Interaction with natural fractures

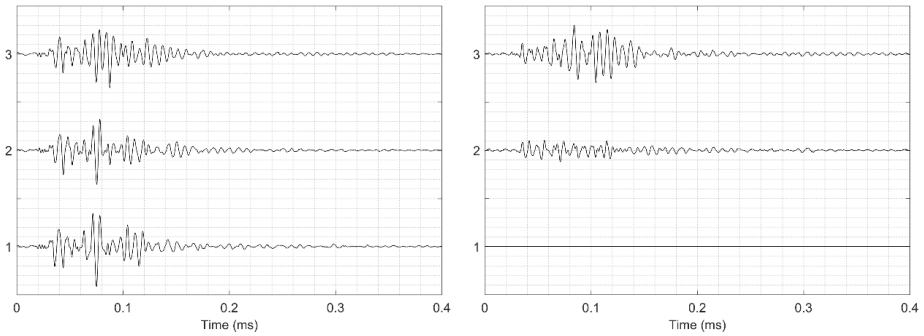

(*d*) Original wave profiles (coal, YD14-ZD10, dS)

(*e*) Processed wave profiles by subtracting the first scan from each subsequent scan (coal, YD14-ZD10, dS)

Fig.10. Interpretation of seismic spectrograms in response to injection to naturally fractured blocks.

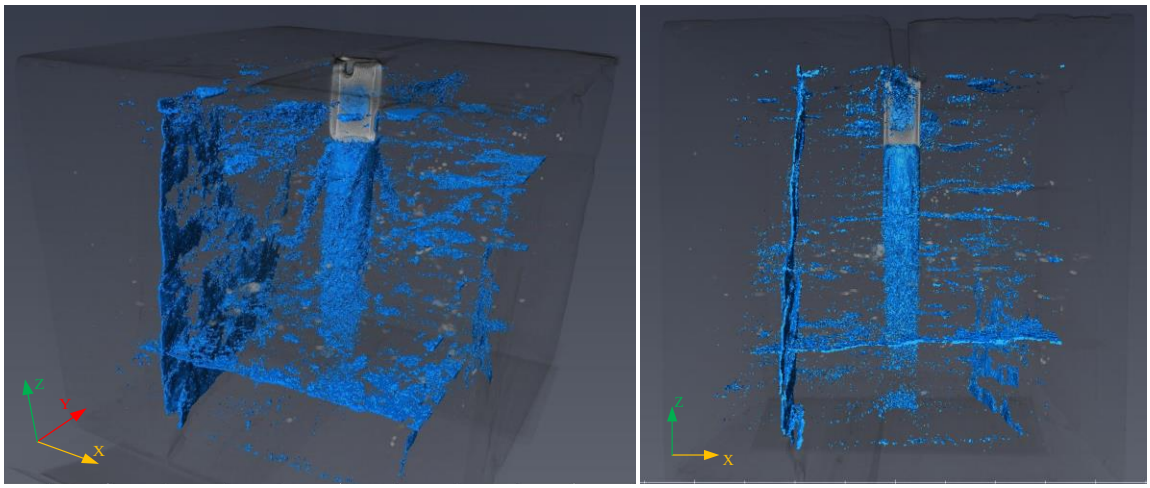

(a) (b)

Fig.11. CT scan of the post-fractured coal block: (a) 3D view, and (b) front view.

4. CONCLUSIONS

Hydraulic fracturing experiments were conducted on 0.3 m cubic samples of relatively homogeneous and intact shale block and a weaker and naturally fractured coal block under true tri-axial stress conditions. Analysis of the seismic response over the hydraulic fracturing process suggested an earlier fracture initiation and interaction between the induced and natural fractures in the coal block when compared with that of the shale block. The induced fracture in the shale block was planar and ran through the whole block, while that in the coal block connected to pre-existing natural fractures shortly after the initiation. Seismic spectrograms of transmission raypaths could only capture the initiation of the induced fracture, while those of diffracted raypaths could reflect both the fracture initiation and its subsequent interactions with the natural fracture system. Results suggested that seismic waves propagating through the fractured coal block experience multiple reflection and diffraction and

become more scattered than those in the relatively intact shale block (Figure 11). Currently new experiments are being conducted and a detailed analysis of the CT images are being carried out to correlate the position of the induced fractures and acoustic signals.

ACKNOWLEDGEMENTS

The first author wishes to thank the Schlumberger Faculty for the Future Fellowship for the support she receives towards her research at Imperial College. The second author acknowledges the UK Engineering and Physical Sciences Research Council (EPSRC) scholarship awarded by the Faculty of Engineering at Imperial College London. The authors wish to thank Karel Heller and Marc Friebel of the Geoscience and Engineering Laboratory, Delft University of Technology and Graham Nash, Gary Jones and Harshit Agrawal of Imperial College London for their contributions to the laboratory experiments throughout the research described in this paper. The authors also thank Alan Porter, the Assistant Quarry Manager at Hope Cement Works UK and Dr Krzysztof Kapusta at Central Mining Institute Poland who have supplied the shale and coal samples used in the project.

REFERENCES

Akrad, O., J. Miskimins, and M. Prasad. 2011. The effects of fracturing fluids on shale rock mechanical properties and proppant embedment. İn *SPE Annual Technical Conference and Exhibition, 30 October-2 November, Denver, Colorado, USA.*

Al Tammar, M.J., and M.M.Sharma. 2017. Effect of geological layer properties on hydraulic fracture initiation and propagation:An Experimental Study. In *SPE Hydraulic Fracturing Technology Conference and Exhibition, 24-26 January, Texas, USA.*

Blanton, T. L. 1982. An experimental study of interaction between hydraulically induced and pre-existing fractures. SPE/DOE In *Unconventional Gas Recovery Symposium, 16-18 May, Pittsburgh, PA.*

Dehghan, A. N., K. Goshtasbi, K. Ahangari, and Y. Jin. 2015. Mechanism of fracture initiation and propagation using a tri-axial hydraulic fracturing test system in naturally fractured reservoirs. *European Journal of Environmental and Civil Engineering.* 20: 560-584.

Ding, W., C. Li, C. Xu, , K. Jiu, W. Zeng, and L. Wu. 2012. Fracture development in shale and its relationship to gas accumulation. *Geoscience Frontiers:* 3, 97–105.

Fisher, K., and N. Warpinski. 2012. Hydraulic-fracture-height growth: Real data. *SPE Production and Operations*, February 2012.

Groenenboom, J. 1998. Acoustic monitoring of hydraulic fracture growth. PhD. Thesis, TU Delft.

Guo,F., N.R.Morgenstern, J.D.Scott. 1993. An experimental Investigation into hydraulic fracture propagation-Part2. single well tests. *Int.J.Rock Mech.Min.Sci.&Geomech.* 30:189-202.

Hou, P., F. Gao, Y. Ju, X. Liang, Z. Zhang, H. Cheng, Y. Gao. 2016. Experimental investigation on the failure and acoustic emission characteristics of shale, sandstone and coal under gas fracturing. J. Nat. Gas Sci. Eng. 35: 211-223.

Huang, B., and J. Liu. 2017. experimental investigation of the effect of bedding planes on hydraulic fracturing under true triaxial stress. *Rock Mech Rock Eng.* 50:2627-2643.

Li, Q., H. Xing, J. Liu, and X. Liu. 2015. A review on hydraulic fracturing of unconventional reservoir. *Petroleum*, 1 (1), 8–15.

Liang, Y., Y. Cheng, Q. Zou, W. Wang, Y. Ma, Q. Li. 2017. Response characteristics of coal subjected to hydraulic fracturing: An evaluation based on real-time monitoring of borehole strain and acoustic emission. *J. Nat. Gas Sci. Eng.* 38: 402–411.

Meng, C., 2010. Intersection between hydraulic fracturing process and pre-existing natural fracture: PhD. Thesis, TU Delft.

Padin, A., A. N. Tutuncu, and S. Sonnenberg. 2014. On the mechanisms of shale microfracture propagation. In *SPE Hydraulic Fracturing Technology Conference, 4-6 February, The Woodlands, Texas, USA.*

Peng,T., J.Yan, H.Bing, Z.Yingcao, Z.Ruxin, C.Zhı, and F.Meng. 2018. Laboratory investigation of shale rock to identify fracture propagation in vertical direction to bedding. *J.Geophys.Eng.*15:696-706.

Savic, M. 1995. Ultrasonic scattering from a hydraulic fracture: theory, computation and experiment. PhD thesis, TU Delft.

Stoeckhert, F., M. Molenda, B.Sebastian, and M.Alber. 2015. Fracture propagation in sandstone and slate-Laboratory experiments, acoustic emissions and fracture mechanics. *Journal of Rock Mechanics and Geotechnical Engineering.* 7:237-249.

Jiang, T., J. Zhang, H. Wu. 2016. Experimental and numerical study on hydraulic fracture propagation in coalbed methane reservoir. *J. Nat. Gas Sci. Eng.* 35: 455-467.

Warpinski, N.R., and L.W. Teufel. 1987. Influence of geologic discontinuities on hydraulic fracture propagation. *J. Pet. Geol.* 39: 209-220.

Van de Ketterij, R.G. 2001. Optimisation of near-wellbore geometry of hydraulic fractures propagating from cased perforated completions. PhD Thesis, TU Delft.

Weijers, L. 1995. The near-wellbore geometry of hydraulic fractures initiated from horizontal and deviated wells. Phd Thesis, TU Delft.

Zhang, J., Kamenov, A., Zhu, D., & Hill, A. D. (2013). Laboratory measurement of hydraulic fracture conductivities in the Barnett shale. *SPE Hydraulic Fracturing Technology Conference*, Woodlands, Texas.

Zhou, J. M. Chen, Y. Jin, and G. Zhang. 2008. Analysis of fracture propagation behavior and fracture geometry using a tri-

axial fracturing system in naturally fractured reservoirs. *Int.J.Rock Mech.Min.Sci*. 45: 1143-1152.

Zhou, J., and X. Chengjin. 2011. Experimental investigation of fracture initiation between natural fractures and hydraulic fractures in naturally fractured reservoirs. In *SPE EUROPEC/EAGE Annual Conference and Exhibition*, 23-29 May, Vienna, Austria.

Zhu, Q., Y. Feng, M. Cai, J. Liu, H. Wang. 2017. Interpretation of the extent of hydraulic fracturing for rockburst prevention using microseismic monitoring data. *J. Nat. Gas Sci. Eng*. 38: 107–119.

Zoback,M., F.Rummel, R.Jung, and C.Raleigh. 1977. Laboratory hydraulic fracturing experiments in intact and pre-fractured rock. *Int.J.Rock Mech.Min.Sci*. 14: 49-58.